Annales Geophysicae, 23, 877–884, 2005
SRef-ID: 1432-0576/ag/2005-23-877

Annales Geophysicae

Evolution of the dispersionless injection boundary associated with substorms

T. Sarris[1,2] **and X. Li**[1]

[1]Lab. for Atmospheric and Space Physics, Univ. of Colorado, Boulder, CO, USA
[2]Demokritus University of Thrace, Xanthi, Greece

Received: 15 July 2004 – Revised: 21 December 2004 – Accepted: 10 January 2005 – Published: 30 March 2005

Abstract. One manifestation of energetic particle acceleration during magnetospheric substorms is the sudden appearance of particle injections into the inner magnetosphere, often observed near geosynchronous orbit. Injections that show simultaneous flux increases in all energy ranges of a detector are called dispersionless injections, and are most often observed in a narrow region around local midnight. In these events it is assumed that the satellite is located close to or inside the region where acceleration and/or transport processes are taking place, called the injection region. We present a study of the location, extent and temporal evolution of the injection region, based on simulation results of a model of the expansion of the electric and magnetic fields associated with a substorm. The model simulates the fields during a substorm onset with an electric field and consistent magnetic field pulse that propagates towards the Earth with a decreasing speed. Our simulation shows that the dispersionless injection boundary can be considered coincident with the leading edge of the pulse field, which transports particles toward the Earth across a certain range of local time. Under the same model field, the dispersionless injection boundary shifts eastward for electrons and westward for protons, consistent with the observation results deduced from statistical analysis of multiple spacecraft measurements.

Keywords. Magnetospheric physics (Storms and substorms) – Space plasma physics (Charged particle motion and acceleration; Numerical simulation studies)

1 Introduction

Injections of energetic particles (tens to hundreds of keV) are among the most important and common aspects of magnetospheric substorms, and, since the time that substorms were first described (Akasofu, 1964), they have been studied extensively (e.g. Arnoldy and Chan, 1969; Baker et al., 1982; Lopez et al., 1990; Reeves et al., 1991; Birn et al., 1997a). However, new and important features keep emerging, in particular as more and more satellites allow for simultaneous multi-point measurements and new modelling efforts provide global pictures of the evolution of substorms. Some of the conclusions of the previous studies of energetic particle injections are the following: 1) Injections are initiated in what is called the acceleration region, where they exhibit a dispersionless character; subsequent drift from the acceleration region produces energy dispersed flux variations (e.g. McIlwain, 1974). 2) Energetic particle injections and magnetic field dipolarization, (i.e. the return of the magnetic field from a stretched to a relaxed state) occur concurrently (Swanson, 1978; Sauvaud and Winckler, 1980). 3) The region where acceleration and/or transport processes are taking place, called the injection region, is localised within limited longitudinal and latitudinal extent (e.g. Belian et al., 1978), and exhibits sharp radial gradients (e.g. Reeves et al., 1991). The existence of a sharp inner front of both the injected accelerated particles and magnetic field dipolarization (injection front) has been confirmed by observation (e.g. Sergeev et al., 1998). 4) There exists a region in which ions and electrons are injected together (central injection region); in the adjacent regions either one species precedes the other or only one species is injected (injection periphery) (Reeves et al., 1991; Birn et al., 1997a). 5) The occurrence frequency of injections has a peak around midnight, with an asymmetry favouring pre-midnight local times (Lopez et al., 1990). 6) During a substorm, the associated fields and flux variations expand earthward (Ohtani, 1998); 7) they start in the midnight sector and expand azimuthally both eastward (into the morning sector) and westward (into the evening sector), as simultaneous multi-satellite observations, combined with data from ground magnetometers have demonstrated (Arnoldy and Moore, 1983; Nagai, 1991; Thomsen et al., 2001).

Many models and interpretations have been proposed over the past 30 years in order to explain the phenomenology of particle injection measurements and in particular their dispersionless nature, sharp gradients and localization. Some of the ideas that have been proposed over the years suggest that: a) transient electric fields rapidly heat and inject particles into a region outside a sharp boundary (McIlwain, 1974), b) a time-dependent shifting of stationary particle boundaries

Correspondence to: T. Sarris
(tsarris@ee.duth.gr)

is occurring (Kivelson, 1980), c) injections are the result of satellite motion through stationary particle distribution (Kivelson et al., 1980), d) a compression-like wave propagates from the tail regions into inner magnetosphere, heating and transporting plasmas as it goes (Moore et al., 1981), e) a stationary injection boundary exists in the nightside magnetosphere, along which particles are accelerated (Mauk and Meng, 1983), f) injections are caused by electric field pulses that are fast magnetosonic waves in nature, radiated by the current disruption region (Sergeev et al., 1998). In the same study, Sergeev et al. (1998) reported that the injection front has a complicated structure, consisting of a diamagnetic hot proton layer followed by the dipolarization front which contains the enhanced energetic electron flux.

Most of the models mentioned above, with the exception of the ones described in Moore et al. (1981) and Sergeev et al. (1998), involve stationary boundaries that separate different plasma populations or different acceleration mechanisms. However, studies involving radially separated satellites have demonstrated a temporal radial expansion of the dispersionless injection region and the dipolarization signatures. For example, Moore et al. (1981), using ATS-6 and SCATHA when they where radially separated, found that particle injections are seen earlier at the satellite that is farther from the Earth, with a 1–10 min time delay for a radial separation of $\sim$1 R_E. Reeves et al. (1996), using LANL and CRRES satellites, extended this observation inside geosynchronous orbit, and calculated the average propagation speed of the injection front at 24 km/s.

Similarly, studies involving azimuthally separated satellites have demonstrated a temporal azimuthal expansion of the dispersionless injection region and the dipolarization signatures. For example, Thomsen et al. (2001), using two-satellite observations of injections at geosynchronous orbit, have shown that the injection regions for both ions and electrons expand azimuthally in both eastward and westward directions over a time scale of several minutes.

The dipolarization of the magnetic field during a substorm that occurs concurrently with energetic particle injections has been associated with the occurrence of earthward fast-flow (or plasma flow burst) events (Nakamura et al., 2002). Fast flows are described as transient flow increases (Bursty Bulk Flows or BBFs), that are responsible for most of the earthward transport of plasma and magnetic flux (Angelopoulos et al., 1992). Statistical studies of the fast flows associated with the substorm expansion phase showed that high-speed convection flows are concentrated in the pre-midnight region (Nagai and Machida, 1998). This local time distribution is consistent with the center of the current wedge region, which was obtained to be located around 23 MLT (Nagai, 1991).

A theoretical model that is a likely candidate for the description of fast flows is one involving plasma-depleted flux-tubes or bubbles proposed by Pontius and Wolf (1990). The existence of plasma bubbles and their association to fast flow events was proven by Sergeev et al. (1996).

Shiokawa et al. (1997) have suggested a mechanism for the braking of the observed fast flows based on statistical observations made by the AMPTE/IRM satellite under which fast flows are decelerated as they propagate earthward by a tailward pressure force. They predict a sudden stop of earthward flows at $<10\,R_E$; however, Sergeev et al. (2000) have shown an event with excellent satellite coverage in which a fast flow event propagates down to $6.6\,R_E$.

Li et al. (1998) have used a model of a transient electromagnetic structure that is shaped as a Gaussian pulse propagating as the compressional wave described by Moore et al. (1981). This model has been used to simulate the observed transient fields during particular substorms, for which it reproduces many features of particle injections at geosynchronous orbit. Later, Sarris et al. (2002) refined the model of Li et al. (1998) to account for the observed deceleration of fast flows and the associated dipolarization signatures, and reproduced the dispersionless injection features at two radially separated satellites. This pulse model shows some resemblance to the features of a plasma bubble.

In the current study, the model of Sarris et al. (2002) is used to determine the location, azimuthal extent and propagation features of the dispersionless injection boundary during the substorm of 27 August 2001. The particular event was observed simultaneously by many satellites and is described in Baker et al. (2002). Some simulation results using the pulse-field model for this event are presented in Li et al. (2003); here we focus instead on the geometric extent and the propagation characteristics of the dispersionless injection boundary. In the following, a brief description of the model is first given, followed by the simulation results and the illustrations of the temporal and spatial variations of the dispersionless injection boundary.

2 Model description

The transient field in the model is associated with the dipolarization process in the magnetotail and is simulated as an electromagnetic Gaussian pulse of localized radial and longitudinal extent which propagates earthward at a decreasing speed. The electric field is purely azimuthal and is strongest at midnight (Li et al., 1998; Sarris et al., 2002). The propagation velocity of the electromagnetic pulse in this model decreases with radial distance as the pulse propagates earthward, in a fashion similar to Sarris et al. (2002), which is consistent with observations where the propagation speed of substorm injections was calculated based on measurements from two radially separated spacecraft (Russell and McPherron, 1973; Moore et al., 1981; Reeves et al., 1996). In the spherical coordinate system (r, θ, ϕ), the electric field is given by:

$$\mathbf{E}_\phi = -\hat{e}_\phi E_0 \left(1 + c_1 \cos\left(\phi - \phi_0\right)\right)^p \exp\left(-\xi^2\right), \qquad (1)$$

where $\xi = [r - r_i + v\,(r)\,(t - t_0)]\,/d$ determines the location of the maximum value of the pulse; $v(r) = a + b \cdot r$ is the pulse-front velocity as a function of radial distance r; d is the width of the pulse; c_1 (>0) and p (>0) describe the local time dependence of the electric field amplitude, which is largest at ϕ_0; $t_a = (c_2\, R_E / v_a)\ (1 - \cos(\phi - \phi_0))$ represents the

delay of the pulse from ϕ_0 to other local times; c_2 determines the magnitude of the delay, v_a is the longitudinal propagation speed of the pulse (assumed constant) and r_i is a parameter in the simulation that determines the arrival time of the pulse. The values of the above parameters that were used in the simulation are: E_0=2mV/m, c_1=1, c_2=0.5 R_E, a=86.0 km/s, b=0.0145 s^{-1}, p=8, v_a=20 km/s, r_i=100 R_E, d=2.8×10^8 m, ϕ_0=160°. No background convection or corotation electric field was included in the model. The convection and corotation electric fields are a dominant factor for the motion of particles in the energy range from eV to tens keV. The LANL and GOES energy channels that we are monitoring in the present study are measuring particles in the 100 keV to 700 keV range. In the simulations we are tracing particles at that energy range.

The consistent magnetic field of the dipolarization process for a given electric field is obtained from Eq. (1) and from Faraday's law, after performing the curl calculation in spherical coordinates and integrating:

$$\boldsymbol{B}_\theta = \hat{e}_\vartheta E_0 \,(1+c_1 cos(\phi-\phi_0))^p \times \left[\frac{1+v'(r)\left(t-t_{ph}\right)}{v(r)} e^{-\xi^2} - \frac{dv'(r)\sqrt{\pi}}{2v(r)^2}\,(1+erf(\xi)) + \frac{d\sqrt{\pi}}{2rv(r)}\,(1+erf(\xi)) \right], \quad (2)$$

where $erf(x) = {}^2/_{\sqrt{\pi}} \int_0^\infty e^{-x^2} dx$ is the error function.

The magnetic field of the pulse, B_θ, is superimposed on a background magnetic field, B_E, which is time-independent. B_E is modelled as a simple dipole field in the present simulation. The pulse field and background field satisfy $\mathbf{E}_\phi \cdot (\mathbf{B}_\theta + \mathbf{B}_E) = 0$ and $\nabla \cdot (\mathbf{B}_\theta + \mathbf{B}_E) = 0$. In the simulation we consider only equatorially mirroring particles, which move on average according to the relativistic guiding center equation described in Northrop 1963):

$$v_d = c\frac{E \times B}{B^2} + \frac{\mu c}{\gamma q}\frac{B \times \nabla_\perp B}{B^2}, \quad (3)$$

where c is the speed of light in a vacuum, e is the electron charge, γ is the relativistic correction factor: $\gamma = (1-v^2/c^2)^{-1/2}$, $\mu = p_\perp^2/2m_0 B$ is the relativistic adiabatic invariant, $p_\perp$ is the particle's perpendicular momentum, m_0 is the particle rest mass, **E** and **B** are the vector electric and magnetic fields in the frame of the particle and $\nabla_\perp$ is the gradient perpendicular to the local magnetic field direction and q is the particle's charge. In the energy range that is considered and for the rate of change of the fields in the model, electrons and protons behave adiabatically (e.g. Li et al., 2003) and Eq. (3) is valid.

3 Model results

We followed a large number of particles (500 000 electrons and 750 000 protons) as they drifted in the equatorial plane in the combined pulse and background fields, recording their initial conditions, final energy, arrival time, and radial distance as they passed various local times. Electrons and protons were initially distributed randomly in radial distance between 4 and 14 R_E and at all local times in the equatorial plane; they were assigned initial energies from 6 keV with a 5% increment, up to 700 keV. In the post-processing stage, each particle is given a weight based on its initial position and energy representing its contribution to the initial distribution. The initial energy distribution was a kappa distribution (Vasyliunas, 1968) with k=1.8 and E_0=0.5 keV for electrons and k=2.7 and E_0=2.5 keV for protons. These parameters are typical for a moderately active plasma sheet (Christon et al., 1991) and similar to the ones used by Birn et al. (1997b, 1998). The initial radial dependence is set according to Li et al. (1998), who used an analytic model to assign a differential flux to each particle:

$$Q_r = \left[\frac{(r_0 - a_0)^{nl}}{r_0^{ml}}\right] \Big/ \left[\frac{(a_{0d} - a_0)^{nl}}{a_{0d}^{ml}}\right], \quad (4)$$

where a_0=3, nl=4, ml=10, a_{0d}=6 for both electrons and protons. For protons, another factor is added: $f_r = f_{r0} * \exp(-r_0^2/9.5^2)$, when r_0 is greater than 9.5 R_E.

Thus, given an initial particle distribution, we can obtain particle fluxes and distributions at any location and time, and compare the simulation results with observations. In Fig. 1, we present electron measurements and model results (upper panels) for a substorm that occurred on 27 August 2001. The measurements, shown in the upper left panels, are GOES-8 electron integral flux (>600 keV) and electron differential fluxes at LANL satellites LANL-97A, 1994–084 and 1991–080, which correspond to numbers 1, 2 and 3, respectively. In the upper right panels, the simulation results are all electron differential fluxes for the four satellite locations, as there was an upper limit in the initial energies of particles that were traced and the construction of integral fluxes was not possible. In the lower panel, a snapshot of particle locations and satellite locations at 04:09 UT is presented; at that time a clear dipolarization signature was observed at the GOES-8 satellite (Baker et al., 2002). Particle energies are colour-coded, from 100 keV (blue) to 800 keV (red). The yellow lines denote the first occurrence of an injection (increase by a factor of >2 in particle fluxes), and the red lines correspond to time 04:09 UT.

The background magnetic field is modeled as a dipole field and thus its magnitude falls as $1/r^3$. The pulse magnetic field has a radial gradient that is dependent on the pulse magnitude and velocity; the expression for the pulse radial gradient is given in Sarris et al. (2002). The local field gradient will depend on the comparison of the gradients of the two superimposed fields. In general, both field configurations have sharper gradients closer to the Earth; however, within the geosynchronous orbit the gradient of the background field dominates for the pulse shape and velocity of our model.

Upon arrival of the propagating pulse the magnetic field gradient is locally reduced or reversed. As a consequence the eastward gradient drift of the electrons and westward

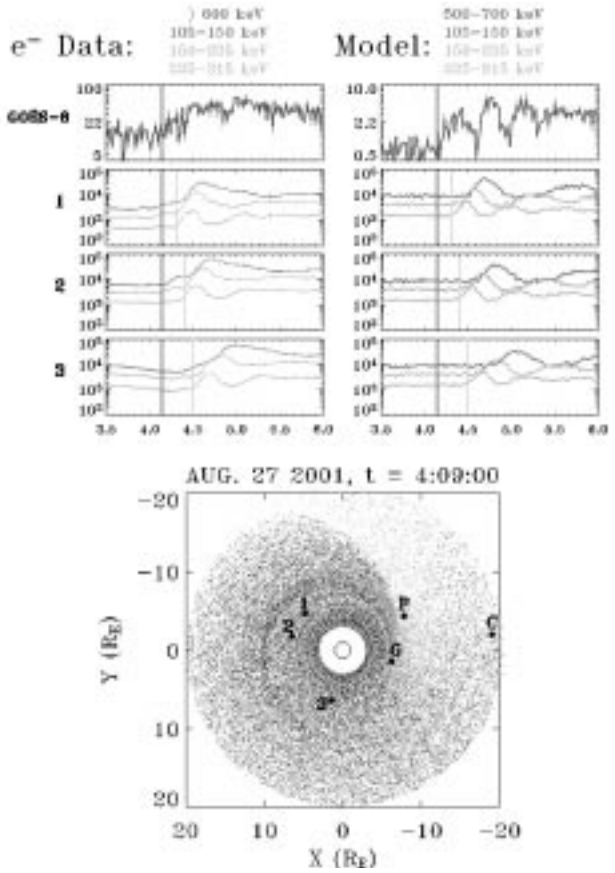

Fig. 1. Flux measurements from GOES-8 (G) and 3 LANL satellites (1, 2 and 3) on 27 August 2001 (upper left) and simulated differential fluxes at the corresponding virtual satellite locations (upper right). On the lower panel, a snapshot of the locations of individual simulated particles at 04:09 UT and satellite locations at that time is presented.

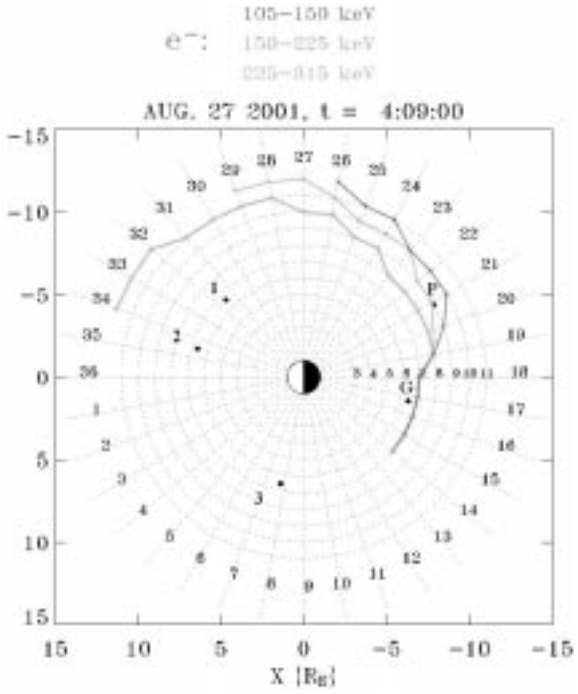

Fig. 2. Locations at which an electron flux increase was observed in the simulation, in the 225–315 keV energy channel (yellow line), 150–225 keV (green) and 105–150 keV (dark blue). At the locations where the three lines coincide the flux increase occurs simultaneously at all three energy channels (electron dispersionless injection boundary).

gradient drift of protons stops and even reverses. This process helps keep the bulk of the ions and electrons together as they are injected earthward and allows particles to be transported to and inside of geosynchronous orbit from tailward of $10\,R_E$. Particles that escape the local region of the transient pulse resume a gradient-B drift, as can be seen from the spiral formation in the lower panel of Fig. 1. At geosynchronous orbit, they are subsequently observed by LANL satellites 1, 2 and 3, with increased dispersion. The electrons in the simulation seem to drift faster and more coherently than the measurements; this is due to the fact that we only trace 90-deg pitch angle particles at the magnetic equator in the simulation, whereas the LANL and GOES flux measurements plotted are omni-directional. In the simulation presented a dispersionless injection would be observed at the location of GOES-8; however, this particular satellite can provide only integral flux measurements, to which we qualitatively compare the simulated differential flux of the highest energy particles traced. The drift-echo features seen in the simulation results (and not in measurement) are due to this finite energy range.

4 Dispersionless injection boundary

In order to calculate the extent of the boundary along which injections appear without energy dispersion (dispersionless injection boundary), we calculate the fluxes for three different energy channels along a grid of locations spaced every 10 deg in azimuth and $1\,R_E$ in radial distance on the equatorial plane for time intervals of 1 min. Increases of the constructed particle fluxes were identified by means of an algorithm that calculated the slope of the time series of constructed particle fluxes at one location. A change in flux was characterised as a particle injection if an increase by a factor of >2 within 2 min was recorded in any single channel. As onset time we chose the start time of the rise in the flux, which is usually better identifiable than the time of the steepest rise. A similar approach was followed by Birn et al. (1997a), who used an automated routine to identify particle injections from LANL data. In Fig. 2 all locations of initial occurrence of an injection were connected graphically by a line for each of the three energy channels for one snapshot of the simulation (04:09 UT). Each line represents the first occurrence of an injection for the given energy channel. Flux increases in the 105–150, 150–225 and 225–315 keV energy channels are connected with a blue, green and yellow line, respectively. At the locations where these three lines coincide, flux increases occur simultaneously at all three energy channels, i.e. along this line dispersionless injections

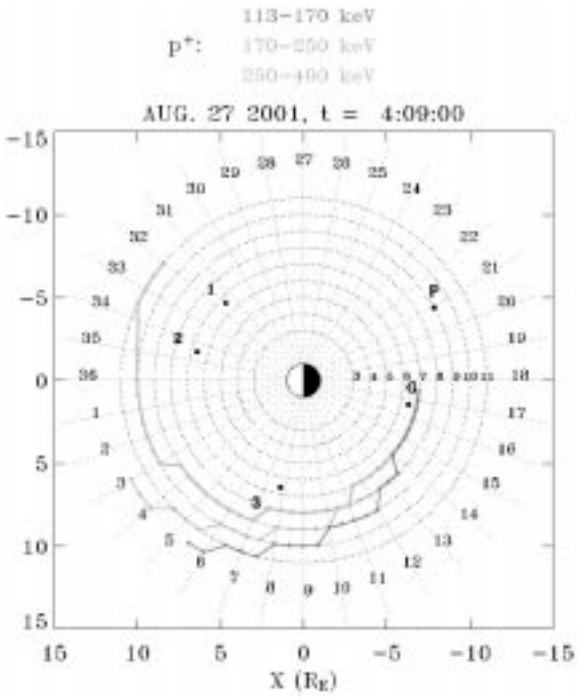

Fig. 3. Locations of initial proton flux increase in the 250–400 keV energy channel (yellow line), 170–250 keV (green line) and 113–170 keV energy channel (dark-blue line) and of the proton dispersionless injection boundary.

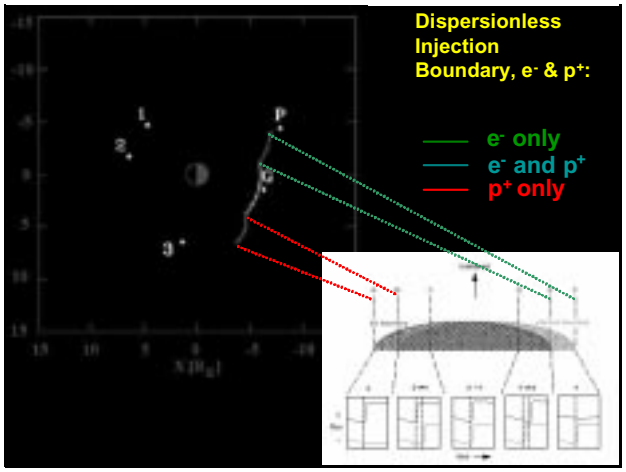

Fig. 4. A snapshot of the superimposed ion and electron dispersionless injection boundary in the simulation is compared to a superposed epoch analysis of particle injections, presented in Plate 2 of Birn et al. (1997a).

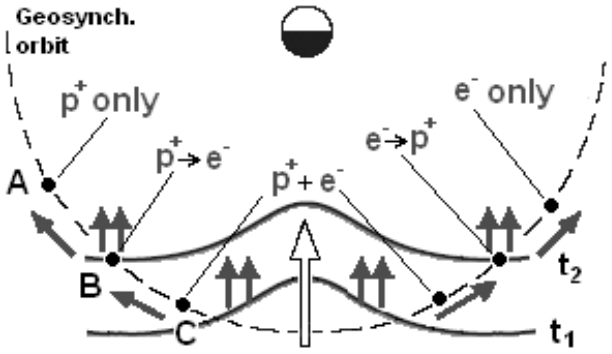

Fig. 5. Schematic of two snapshots of a double-spiral formation of the pulse front. The twin red-green arrows denote electrons and ions that propagate at the front of the pulse without dispersion. The single red (green) arrows denote ions (electrons) that drift out of the zero-grad-B region. Virtual geosynchronous satellites A, B and C will observe ion injections only, ion injections followed by delayed electron injection ($p^+ \rightarrow e^-$), and simultaneous ion and electron injections ($p^+ + e^-$), respectively.

are observed. Hence, this line can be referred to as the "electron dispersionless injection boundary". In a similar fashion, proton flux increases were calculated; in Fig. 3 the injection boundaries for three proton energy channels are presented, along with the "proton dispersionless injection boundary".

5 Ion – electron separation

In Fig. 4 the electron dispersionless injection boundary is plotted together with the proton dispersionless injection boundary for one snapshot of the simulation. From this figure we can see that the two boundaries are azimuthally offset, due to the eastward drift of electrons and the westward drift of protons. In this figure the region of the dispersionless injection boundary where only ion injections occurred (westward edge) is marked in red; the region of simultaneous ion and electron injection is marked in blue and the region of electron injection only (eastward edge) is marked in green. As it can also be inferred from Figs. 1 and 2, the electron dispersionless injection boundary has a sharp westward edge, as electrons cannot propagate further west, and a not-so-sharp eastward edge, as the pulse magnetic field gradient gradually relaxes, allowing electrons to gradually perform a combined inward ($\boldsymbol{E}\times\boldsymbol{B}$) and eastward (grad-B) drift, until they drift away from the influence of the pulse to regions where only dispersed injections can be observed.

The existence of single-species dispersionless injections at the westward and eastward edges of the injection region, called the "injection periphery region", has been noted by Reeves et al. (1991), and was further established by Birn et al. (1997a), who used a superposed epoch analysis of energetic particle fluxes at geosynchronous orbit in order to bring out the dominant and persistent features of particle injections. They found that in addition to an injection periphery region there were regions in which both electrons and ions showed dispersionless injections but that one was delayed with respect to the other and that the five regions (ions only, delayed electrons, simultaneous electrons and ions, delayed ions, and electrons only) were well-ordered in local time. The results are shown schematically in the inset of Fig. 4, (Plate 2 of Birn et al. (1997a)), in which particle injections are classified into 5 categories: ion injections only, ion

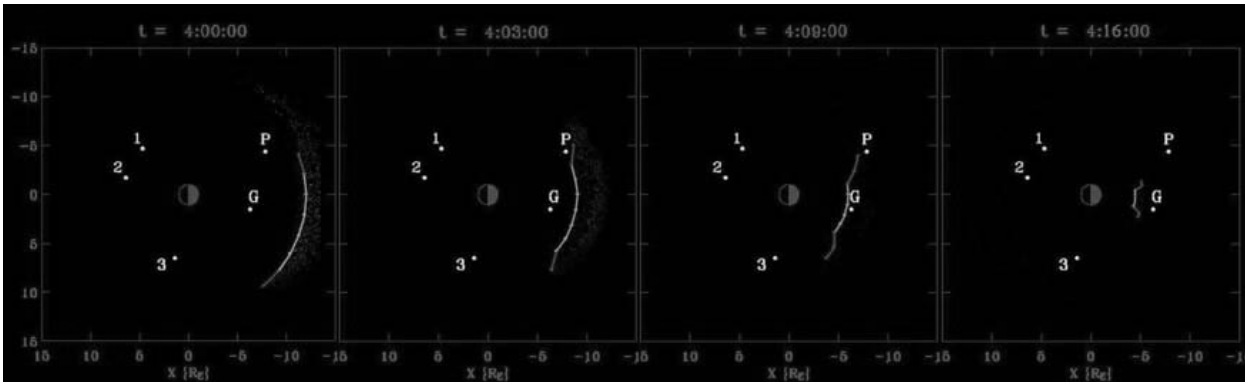

Fig. 6. Snapshots of the superimposed ion and electron dispersionless injection boundary in the simulation.

injections followed by delayed electron injection ($p^+ \rightarrow e^-$), simultaneous ion and electron injections ($p^+ + e^-$), electrons followed by ions ($e^- \rightarrow p^+$) and electron injections only.

The comparison between the simulated injection boundary presented herein and the epoch analysis of Birn et al. (1997a) yields a consistent picture; however, no $p^+ \rightarrow e^-$ or $e^- \rightarrow p^+$ delayed injections have been observed in the model results. Such delayed injections could be observed if the model implemented a double-spiral formation of the injection front that has been described, for example, in Konradi et al. (1974). Two snapshots of such a formation for the pulse front are presented in Fig. 5. Along the front of the pulse electrons and protons are energized simultaneously at the region of reduced or even reversed grad-B, as described above. However, particles that gain energy at the pulse front may escape the local gradient-reversal region of the transient pulse and resume their gradient-B drift, which is faster than the propagation velocity of the pulse. In the double-spiral pulse-front formation given in the schematic of Fig. 5 protons that resume a grad-B drift (single red arrows) will reach virtual satellite B and subsequently satellite A, producing injections that will appear dispersionless, due to the close proximity of the satellites to the injection front. When the pulse front reaches satellite B both electron and proton injections occur (twin red-green arrows), thus producing the $p^+ \rightarrow e^-$ delayed signature. At virtual satellite A no electron injections will be recorded, as it lies beyond the azimuthal extent of the injection front, which exhibits sharp radial gradients according to observation (e.g. Reeves et al., 1991).

The double-spiral formation could be introduced in the model by assuming a slower azimuthal propagation of the pulse (parameter c_2 in Sect. 2); however, no observational constraints could be used in this event to control the azimuthal expansion of the pulse fields.

In Fig. 6 the injection boundary is plotted for 4 snapshots of the simulation. It can be seen that, according to this model, the dispersionless injection boundary follows the pulse front as particles of all energies are first energized at the front of the pulse electric field, which is consistent with CRRES observations showing the occurrence of dispersionless injections down to L=4.2 R_E.

6 Discussion – Conclusions

Since electrons and ions have oppositely directed gradient-curvature drifts, if the earthward injection requires a finite propagation time, then a separation of the two species is expected. This was one of the key factors which led to models that involved stationary boundaries and implied that the source region for substorm injections was located outside – but not far outside – geosynchronous orbit, where most observations of injections were made. However, in the simulations presented, the propagating pulse that simulates the dipolarization field locally reverses the magnetic field gradient of 90° pitch angles and therefore can reduce or reverse the gradient drift at larger radial distances. This process helps keep the ions and electrons together as they are injected earthward by $\boldsymbol{E} \times \boldsymbol{B}$ drift due to the electric field of the pulse. The local reversal of the gradient is also what allows particles of different energies to be transported without significant dispersion to 6.6 R_E from tailward of 10 R_E (see Sarris et al. (2002); Li et al. (2003)), where the simulations of Birn et al. (1997b, 1998) and the observations of Fairfield et al. (1998) show that the effects of flow bursts are strongest. Thus, dispersionless injections for both species are observed along a transient earthward-propagating dispersionless injection boundary; this boundary is located at the leading edge of the transient earthward electromagnetic field associated with the dipolarization process, since it is in this region that grad-B reversal occurs.

The observed separation in local time of the ion and electron injection regions has been explained by Birn et al. (1998) as the result of the earthward propagation of two azimuthally separated injection fronts for ions and electrons. In the work presented herein, a separation of three regions along the dispersionless injection boundary (p^+−only, e^-−only and simultaneous $e^- - p^+$ injections) was demonstrated to occur at the leading edge of the earthward pulse; this separation was explained in terms of a gradual drift (eastward for electrons, westward for protons) out of the grad-B reversal region. Under this model, $p^+ \rightarrow e^-$ and $e^- \rightarrow p^+$ delayed injections have not been observed; however, a pulse that is reflected about midnight to form a double spiral, such as

described in Konradi et al. (1974), could produce such delayed injections.

One conclusion that we can draw from the simulation that was performed is that the effects of the injection are global: from the extent of the spiral lines that indicate flux enhancements in Figs. 2 and 3 and from the extent of the region of depleted source population that was discussed above, we can see that the occurrence of flux increases or decreases extend well beyond and within the geosynchronous orbit (see Fig. 6).

Using a simple model it was shown that the dispersionless injection boundary propagates through a continuous region, it is not stationary, and energizes and transports particles as it goes. A slightly different concept has been suggested before by Moore (1986), who proposed that the magnetosphere is typically configured so as to produce wave braking near synchronous orbit, without explicit reference to the cause of the braking. In another description, Shiokawa et al. (1997) attribute the braking of high-speed flows to the balance between an earthward magnetic tension force and a tailward pressure force; they suggest that these flows are stopped at a clear boundary between the regions of dipolar field (high-pressure gradient) and tail-like field (low-pressure gradient) in the plasma sheet.

Our model does not rule out a preferential radial/azimuthal location over which dispersionless injections occur, perhaps with more evident flux increases: It was demonstrated in Sarris et al. (2002) that a slow-moving, faster-decelerating pulse will exhibit sharper gradients and will thus be more effective in accelerating and transporting inwards energetic particles. If the physical equivalent of the pulse-field model is an inward-propagating fast flow in the form of a plasma bubble, such as described above, then it would brake due to the balance between an earthward magnetic tension force and a tailward pressure force, $-\nabla P_T$, (Shiokawa et al., 1997), where the total pressure, P_T is given by: $P_T = B^2/2\mu_0 + n_i k T_i$, where B is the magnetic field intensity, k is the Boltzmann constant, T_i is the ion temperature and n_i is the ion density. Thus, a sharp increase in the ion density and/or the magnetic field would cause a sudden compression in the plasma bubble, which would correspond to a sudden increase in the magnitude and the gradients of the pulse electric and magnetic fields. This increase would result in increased occurrence rates and intensity of the dispersionless injections over that particular transition region. However, more observational constraints are needed, with more than two radially separated spacecraft, in order to determine and model the braking process of fast flows and the associated dispersionless injection boundary.

Acknowledgements. Support for this work was provided partly by the "Pythagoras" 1249-4 grant and partly by NASA grants (NAG5-13135 and -13518) and NSF grants (CISM, ATM-0233302 and -0101351).

Topical Editor T. Pulkkinen thanks D. Delcourt and another referee for their help in evaluating this paper.

References

Akasofu, S.-I.: The development of the auroral substorm, Planet. Space Sci., 12, 273–282, 1964.

Angelopoulos, V., Baumjohann, W., and Kennel, C. F. et al.: Bursty bulk flows in the inner plasma sheet, J. Geophys. Res., 97, 4027–4039, 1992.

Arnoldy, R. L. and Moore, T. E.: The longitudinal structure of substorm injections at synchronous orbit, J. Geophys. Res., 88, 6213–6220, 1983.

Arnoldy, R. L. and Chan, K. W.: Particle substorms observed at the geostationary orbit, J. Geophys. Res., 74, 5019–5028, 1969.

Baker, D. N., Fritz, T. A., and Wilken, B., et al.: Observations and modelling of energetic particles at synchronous orbit on 29 July 1977, J. Geophys. Res., 87, 5917–5932, 1982.

Baker, D. N., Peterson, W. K., and Eriksson, S. et al.: Timing of magnetic reconnection initiation during a global magnetospheric substorm onset, Geophys. Res. Lett., 29(24), 2190, doi:10.1029/2002GL015539, 2002.

Belian, R. D., Baker, D. N., Higbie, P. R., and Jones Jr., E. W.: High resolution energetic particle measurements at 6.6 Re, 2, High-energy proton drift echoes, J. Geophys. Res., 83, 4857–4862, 1978.

Birn, J., Thomsen, F., Borovsky, J. E., Reeves, G. D., McComas, D. J., and Belian, R. D.: Characteristic plasma properties during dispersionless substorm injections at geosynchronous orbit, J. Geophys. Res., 102, 2309–2324, 1997a.

Birn, J., Thomsen, F., Borovsky, J. E., Reeves, G. D., McComas, D. J., and Belian, R. D.: Substorm ion injections: Geosynchronous observations and test particle orbits in three-dimensional dynamic MHD fields, J. Geophys. Res., 102, 2325–2341, 1997b.

Birn, J., Thomsen, F., and Borovsky, J. E. et al.: Substorm electron injections: Geosynchronous observations and test particle simulations, J. Geophys. Res., 103, 9235–9248, 1998.

Christon, S. P., Williams, D. J., and Mitchell, D. G.: Spectral characteristics of plasma sheet ion and electron populations during disturbed geomagnetic conditions, J. Geophys. Res., 96, 1–22, 1991.

Fairfield, D. H., Mukai, T., and Lui, A. T. Y. et al.: Geotail observations of substorm onset in the inner magnetotail, J. Geophys. Res., 103, 103–117, 1998.

Friedel, R. H. W., Korth, A., and Kremser, G.: Substorm onset observed by CRRES: Determination of energetic particle source region, J. Geophys. Res., 101, 13 137–13 154, 1996.

Kivelson, M. G., Kaye, S. M., and Southwood, D. J.: The physics of plasma injection events, in Dynamics of the Magnetosphere, edited by: Akasofu, S.-I., D. Reidel, Norwell Mass., 385, 1980.

Konradi, A., Semar, C. L., and Fritz, T. A.: Substorm-injected protons and electrons and the injection boundary model, J. Geoph. Res., 80, 543–553, 1974.

Li, X., Baker, D. N., Temerin, M., Reeves, G. D., and Belian, R. D.: Simulation of dispersionless injections and drift echoes of energetic electrons associated with substorms, Geophys. Res. Lett., 25, 3763–3766, 1998.

Li, X., Sarris, T. E., Baker, D. N., and Peterson, W. K.: Simulation of energetic particle injections associated with a substorm on August 27, 2001, Geophys. Res. Lett., 30, 1004–1008, doi:10.1029/2002GL015967, 2003.

Li, X., Baker, D. N., and Elkington, S. et al.: Energetic particle injections in the inner magnetosphere as a response to an interplanetary shock, J. Atmos. S.-P., 65, 233–244, 2003.

Lopez, R. E., Sibeck, D. G., McEntire, R. W., and Krimigis, S. M.:

The energetic ion substorm injection boundary, J. Geophys. Res., 95, 109–117, 1990.

Mauk, B. H. and McIlwain, C. E.: Correlation of Kp with the substorm-injected plasma boundary, J. Geophys. Res., 79, 3193, 1974.

Mauk, B. H. and Meng, C.-L.: Characterization of geostationary particle signatures based on the "injection boundary" model, J. Geophys. Res., 88, 3055–3071, 1983.

McIlwain, C. E.: Substorm injection boundaries, in Magnetospheric Physics, edited by McCormac, B. M., 143, D. Reidel, Norwell, Mass., 1974.

Moore, T. E., Arnoldy, R. L., Feynman, J., and Hardy, D. A.: Propagating substorm injection fronts, J. Geophys. Res., 86, 6713–6726, 1981.

Moore, T. E.: Acceleration of low-energy magnetospheric plasma, Advances in Space Research (ISSN 0273-1177), 6, 103–112, 1986.

Nagai, T.: An empirical model of substorm-related magnetic field variations at synchronous orbit, in Magnetospheric Substorms, Geophys. Monogr., 64, ed. Kan, J. R., Potemra, T. A., Kokubun, S., Iijima, T., 91–95, 1991.

Nagai, T. and Machida, S.: Magnetic reconnection in the near-Earth magnetotail, in New perspectives on the Earth's magnetotail, Geophys. Monogr., (Ed.) Nishida, A., Baker, D. N., Cowley, S. W. H., 105, 211–224, 1998.

Nakamura, R., Baumjohann, W., and Klecker, B. et al.: Motion of the dipolarization front during a flow burst event observed by Cluster, Geophys. Res. Lett., 20, 1942, doi:10.1029/2002GL015763, 2002.

Northrop, T. G.: The Adiabatic Motion of Charged Particles, 29, Wiley-Interscience, New York, 1963.

Ohtani, S.: Earthward expansion of tail current disruption: Dual-satellite study, J. Geophys. Res., 103, 6815–6825, 1998.

Pontius, D. H. and Wolf, R. A.: Transient flux tubes in the terrestrial magnetosphere, Geophys. Res. Lett., 17, 49–52, 1990.

Reeves, G. D., Henderson, M. G., McLachlan, P. S., Belian, R. D., Friedel, R. H. W., and Korth, A.: Radial propagation of substorm injections, in Proceedings of ICS-3, Versailles, France, 12–17 May 1996, ESA SP-389, 579–584, 1996.

Reeves, G. D., Belian, R. D., and Fritz, T.: Numerical tracing of energetic particle drifts, J. Geophys. Res., 96, 13 997–14 008, 1991.

Russell, C. T. and McPherron, R. L.: The magnetotail and substorms, Space Sci. Rev., 15, 205–266, 1973.

Sarris, T. E., Li, X., Tsaggas, N. P., and Paschalidis, N. P.: Modeling Energetic Particle Injections in Dynamic Pulse Fields with Varying Propagation Speeds, J. Geophys. Res., 107, doi:10.1029/2001JA900166, 2002.

Sauvaud, J. A. and Winckler, J. R.: Dynamics of plasma, energetic particles and fields near synchronous orbit in the nighttime sector during magnetospheric substorms, J. Geophys. Res., 85, 2043–2056, 1980.

Sergeev, V. A., Angelopoulos, V., and Gosling, J. T. et al.: Detection of localized, plasma-depleted flux tubes or bubbles in the midtail plasma sheet, J. Geophys. Res., 101, 10 817–10 826, 1996.

Sergeev, V. A., Shukhtina, M. A., Rasinkangas, R., Korth, A., Reeves, G. D., Singer, H. J., Thomsen, M. F., and Vagina, L. I.: Event study of deep energetic particle injections during substorm, J. Geophys. Res., 103, 9217–9234, 1998.

Sergeev, V. A., Sauvaud, J. A., and Popescu, D. et al.: Multiple-spacecraft observation of a narrow transient plasma jet in the Earth's plasma sheet, Geophys. Res. Lett., 27, 851–854, 2000.

Shiokawa, K., Baumjohan, W., and Haerendel, G.: Braking of high-speed flows in the near-Earth tail, Geophys. Res. Lett., 24, 1179–1182, 1997.

Swanson, R. L.: Electron intensity and magnetic field changes at synchronous orbit for the auroral electrojet, M. S. thesis, Univ. of Minn., Mineapolis, 1978.

Thomsen, M. F., Birn, J., Borovsky, J. E. et al.: Two-satellite observations of substorm injections at geosynchronous orbit, J. Geophys. Res., 106, 8405–8416, 2001.

Vasyliunas, D. J.: A survey of low-energy electrons in the evening sector of the magnetosphere with OGO 1 and OGO 3, J. Geophys. Res., 73, 2839–2885, 1968.